J. Chem. Sci. Vol. 127, No. 4, April 2015, pp. 717–728.
DOI 10.1007/s12039-015-0828-8

Ethylene homo- and copolymerization chain-transfers: A perspective from supported $(^{n}BuCp)_2ZrCl_2$ catalyst active centre distribution

MUHAMMAD ATIQULLAH[a,*], MAMDOUH A AL-HARTHI[b], SIRIPON ANANTAWARASKUL[c] and ABDUL-HAMID M EMWAS[d]

[a]Center for Refining and Petrochemicals, Research Institute, King Fahd University of Petroleum & Minerals, Dhahran 31261, Saudi Arabia

[b]Department of Chemical Engineering, King Fahd University of Petroleum & Minerals, Dhahran 31261, Saudi Arabia

[c]Department of Chemical Engineering, Kasetsart University, Jatujak, Bangkok 10900, Thailand

[d]NMR Core Laboratory, King Abdullah University of Science & Technology, Thuwal 23955-6900, Saudi Arabia

e-mail: matiq@kfupm.edu.sa

MS received 15 May 2014; revised 7 October 2014; accepted 30 October 2014

Abstract. Polymerization chain termination reactions and unsaturation of the polymer backbone end are related. Therefore, in this study, the parameters resulting from the modelling of the active centre distribution of the supported catalyst—silica/MAO/$(^{n}BuCp)_2ZrCl_2$—were applied to evaluate the active-centre-dependent ethylene homo- and copolymerization rates, as well as the corresponding chain termination rates. This approach, from a microkinetic mechanistic viewpoint, elucidates better the 1-hexene-induced positive comonomer effect and chain transfer phenomenon. The kinetic expressions, developed on the basis of the proposed polymerization mechanisms, illustrate how the active site type-dependent chain transfer phenomenon is influenced by the different apparent termination rate constants and momoner concentrations. The active centre-specific molecular weight M_{ni} (for the above homo- and copolymer), as a function of chain transfer probability, p_{CT_i}, varied as follows: $log\left(p_{CT_i}\right) = log(mw_{ru}) - log(M_{ni})$ where mw_{ru} is the molecular weight of the repeat unit. The physical significance of this finding has been explained. The homo- and copolymer backbones showed all the three chain end unsaturations (vinyl, vinylidene, and trans-vinylene). The postulated polymerization mechanisms reveal the underlying polymer chemistry. The results of the present study will contribute to develop in future supported metallocene catalysts that will be useful to synthesize polyethylene precursors having varying chain end unsaturations, which can be eventually used to prepare functional polyethylenes.

Keywords. Metallocene catalyst; MWD and CCD deconvolution; active centre distribution; ethylene-1-hexene chain end unsaturation; chain termination probability.

1. Introduction

The judicious tailoring of metallocene structures produces well-defined polyolefin microstructures that range from atactic to stereoregular and stereoblock poly(α-olefins). Because of these versatile capabilities of metallocenes regarding the mechanism of olefin polymerization, and the precatalyst structure versus polymer backbone and property relation, our current knowledge exceeds what was known before. So far as the polymerization mechanism is concerned, the termination step governs chain transfer which controls polymer molecular weight and its distribution and chain end structures. Notably, the backbone terminal vinyl offers ample opportunities for synthesizing new materials, particularly functional polyolefins that have special applications. More precisely, vinyl-terminated polyethylenes are potential precursors for chain-end functionalized polyethylenes.[1,2] Additionally, the chain end unsaturations are the nuclei for generating free radicals. Therefore, they significantly affect polymer degradation during processing and outdoor uses of the final products.[3]

As explained above, the investigation of chain transfer phenomenon is a fundamentally important subject. Therefore, we shall review the pertinent literature that, in this regard, concerns ethylene homo- and ethylene-1-hexene copolymerization, using particularly unsupported metallocenes. Several reports confirm the generation of only vinyl and *trans*-vinylene chain-ends during homopolymerization.[4–11] However, during ethylene-1-hexene copolymerization, the situation differs. All the

*For correspondence

three chain-end unsaturations—vinyl (CH_2 =CHR), trans-vinylene (R_1CH=CHR_2, $R_1 \neq R_2$), and vinylidene (CH_2=CR_1R_2, $R_1 \neq R_2$)—are formed.[7,8,12] In each case, suitable chain-end formation mechanism has been postulated in the literature. We, surprisingly, observe that the subject of chain-end unsaturation for supported metallocene-catalyzed ethylene homo- and ethylene-α-olefin copolymerization including 1-hexene, has not been addressed at all. This observation, combined with the industrial importance and scientific research interest in supported metallocenes, makes the background of this study. This is elaborated below.

Supported catalysts are a prerequisite to attaining the desired polymer particulate morphology by the industrial production plants. On the other hand, the supported catalyst olefin polymerization generally differs from the unsupported analogue because of the following: (i) Disintegration of the catalyst particles;[13–16] (ii) Heat, mass-transfer, and sorption limitations; (iii) Catalyst active centre distribution, particularly in the presence of a multi-structured co-catalyst with multiple Lewis acidities; (iv) Electronic effect and steric bulk of the supported catalyst ion-pair gaps; and (v) Varying coordination environments of the metallocene transition metal.

We, therefore, conclude that to study the chain transfer of supported metallocene-catalyzed ethylene homo- and ethylene-1-hexene copolymerization, especially from the perspective of catalyst active centre distribution, is scientifically interesting and worthwhile. To the best of our knowledge, this has not been addressed so far as we propose in this study. This will eventually add a new insight to this subject and broaden our comprehension.

Metallocenes can be generally supported using several immobilization procedures, which have been discussed by Severn and Chadwick.[17] It turns out that silica/methylaluminoxane (MAO) cocatalyst/zirconocene, in general, offers higher catalyst activity than the remaining routes. Therefore, in this study, we synthesized a representative supported metallocene catalyst, namely silica/MAO/$(^nBuCp)_2ZrCl_2$. During polymerization, we did not separately feed MAO to achieve the following: (i) Prevent the associated catalyst leaching and reactor fouling; (ii) Suppress competitive co-diffusion of MAO and ethylene from the polymerization medium to the catalyst active centres; and (iii) Minimize the potential of chain transfer to the MAO cocatalyst.

We used silica as the support because of its stability at high temperatures, availability with varying pore sizes, volumes, and surface areas, low price and very large usage by the industry.[18] We selected $(^nBuCp)_2ZrCl_2$ because of its stability, commercial availability with reasonable price, capability of polymerizing ethylene with high activity in solution, and considerable application to synthesize supported metallocene catalysts.[19–23]

We recently modelled the catalyst active centre distribution of the above supported metallocene catalyst by simultaneous deconvolution of the measured molecular weight and copolymer composition distributions of the resulting polyethylenes, and confirmed the model prediction experimentally (using the differential scanning calorimetry-based successive self-nucleation and annealing (SSA) technique) as well as from the perspective of MAO structural heterogeneity.[24] Models combined with experiments effectively illustrated how and why active centre distribution and the variance in the design of the supported MAO anion, having different electronic and steric effects and coordination environments, influence the concerned copolymerization mechanism and polymer properties, including inter- and intra-chain compositional heterogeneity and thermal behaviour.

In view of the previous discussions, we organize this study to investigate in detail the effects of the aforesaid catalyst active centre distribution on ethylene homo- and ethylene-1-hexene copolymerization chain transfers, including the chain end unsaturation and comonomer effects.

In this report, we particularly focus on chain transfer from the perspective of catalyst active centre distribution. However, the approach reported in the present work can be easily extended to look into this subject considering the other factors listed above.

2. Experimental

This section deals with materials used in this study, synthesis of the supported catalyst and determination of catalyst elemental composition, synthesis of polyethylenes and their characterization. Table 1 lists the elemental composition of the synthesized catalyst and its polymerization productivities for ethylene homo- and copolymerization.

The polymer characterization includes weight average molecular weight M_w and polydispersity index (PDI), polymer material density, bulk thermal properties (peak melting point, peak crystallization point, and % crystallinity), thermal fractionation, copolymer composition distribution, average copolymer composition, and chain end vinyl unsaturation. Table 2 summarizes the aforesaid properties of the as-synthesized ethylene homo- and copolymer.

Table 1. Elemental composition of the synthesized supported catalyst and its polymerization productivities.[24]

Catalyst composition and productivity	Units	Experimental values for the synthesized supported catalyst
Silicon (Si)	wt %	28.43
Aluminum (Al)	wt %	67.78
Zirconium (Zr)	wt %	3.70
Al:Zr molar ratio	Dimensionless	61.89:1.00
Homopolymerization productivity	kg PE/g cat h $\times 10^2$	20.0
Copolymerization productivity	kg PE/g cat h $\times 10^2$	52.5

Polymerization conditions: medium = n-hexane, 240.0 mL; 1-hexene = 10.0 mL; Scavenger = 1.0 mL; 1.0 M TIBA; Temperature = 50°C; Mode of polymerization trial: continuous feeding of ethylene at 5 bar(g).

Table 2. Properties of the synthesized ethylene homo- and copolymer.[24,25]

Itemized polymer properties	Units	Experimental values for Homopolymer	Copolymer
Weight average molecular weight M_w	g mol^{-1}	166,678	74,435
Polydispersity index PDI	Dimensionless	5.496	3.8152
Polymer material density ρ^a_{polym}	g mL^{-1}	0.969	0.913
Peak melting point T_{pm}	°C	133.30	118.07
Peak crystallization point T_{pc}	°C	116.01	105.24
Crystallinity X_c	%	79.60	43.69
Breadth of *Crystaf* composition distribution $T_{\sigma Crystaf}$	°C		9.23
Average 1-hexene composition	mol%		2.51
Terminal vinyl $\times 10^3 CH_2$ =CHR	Number per 1,000 C	0.16363	0.12014
Vinylidene $\times 10^3 CH_2$ =CR_1R_2; $R_1 \neq R_2$	Number per 1,000 C	0.07153	1.90753
trans-vinylene $\times 10^3$ R_1CH=CHR_2; $R_1 \neq R_2$	Number per 1,000 C	1.18842	0.67355
Total vinyl unsaturation $\times 10^3$	Number per 1,000 C	1.42358	2.70122

[a]Calculated using the rule of additivity of volumes of amorphous and crystalline phases, and DSC-determined fractional crystallinity (X_c) : $X_c = (1/\rho_{polym} - 1/\rho_a)/(1/\rho_c - 1/\rho_a)$; ρ = density; a = amorphous phase; c = crystalline phase; polym = polymer. For polyethylene, $\rho_c = 1.004$ g/mL and $\rho_a = 0.853$ g/mL.

The procedures related to what has been stated above have been detailed in our recent publications.[24,25]

2.1 *Modelling of catalyst active centre distribution*

The catalytic synthesis of ethylene homo- and copolymers (with an α-olefin) is implicitly a statistical process. Consequently, the polymer backbones consist of a mixture of chains that can be represented by various single-site molecular weight distributions (MWDs) and copolymer composition distributions (CCDs). Therefore, the deconvolution of the measured MWDs and CCDs—an inverse computational technique—can determine the number of active catalyst site types, that is, the catalyst active center distribution and model the corresponding backbone microstructures (MWD and CCD). The mathematical development of the aforesaid deconvolution model and the associated computational algorithm are detailed in the literature.[24–29]

3. Results and Discussion

In this section, we address the following three subjects from the viewpoint of active centre types of the supported catalyst silica/MAO/(^{n}BuCp)$_2$ZrCl$_2$: (i) Catalytic activity and comonomer effect; (ii) Number average molecular weight M_{ni}; and (iii) Polymer backbone end unsaturation.

We obtained the catalyst active site type-specific number average molecular weight M_{ni} from the simultaneous deconvolution of MWD and CCD of the as-synthesized polyethylenes (table 3).[24,25]

Table 3. Catalyst site types and the estimated deconvolution model parameters.[24,25]

Polymer type	Model parameters	Active catalyst site types				
		1	2	3	4	5
Homopolymer	$\chi^2 \times 10^3$			2.83		
	m_i	0.0377	0.1638	0.3346	0.3602	0.1038
	M_{ni} (g/mol)	12,583	59,668	178,504	445,576	1,283,822
Copolymer	$\chi^2 \times 10^3$			7.05		
	m_i	0.0760	0.2312	0.3329	0.0900	0.2699
	M_{ni} (g/mol)	3,088	17,707	42,097	51,375	109,525

Figure 1 compares the copolymerization versus homopolymerization rates of the predicted catalyst active site types. We calculated these rates as reported in the literature.[30] First, we observe that different active sites showed different homo- as well as copolymerization rates. We also derive, $R_{p,homopolym}$ and $R_{p,copolym}$. See Equations A24 and A31, respectively (Appendix A).[11,17,19,31–44] These equations show how they correlate to the different apparent propagation rate constants and the momoner concentrations. Second, we note that each active site type copolymerization rate is higher than the corresponding ethylene homopolymerization rate. This signifies that each active site type effectively demonstrated varying rate enhancement (positive comonomer) effects, which can be assessed as follows: Active site type 2 > Active site type 1 > Active site type 3 > Active site type 4 > Active site type 5.

Figure 2 exhibits that the active site type-dependent number average molecular weights are related to the respective homo- and copolymerization rates. This relation, based on catalyst active centre distribution, is approximately reverse. However, this dependence varied with polymerization type. The impact is more pronounced in copolymerization than in homopolymerization.

Figure 3 demonstrates how the copolymer active site type number average molecular weight M_{ni} dropped with respect to the homopolymer analogue. The common observation is that the values of M_{ni} differed from site to site. We note that Active sites 3, 4, and 5 were more effective in decreasing the molecular weight (due to the feeding of 1-hexene) than Active sites 1 and 2. Therefore, the chain transfer reactions occurred more strongly in Active sites 3, 4, and 5 than in Active sites 1 and 2. The efficacy of chain transfer can be ranked as: Active site type 5 > Active site type 4 > Active site type 3 > Active site type 2 > Active site type 1. Now, we address the kinetic perspective of this finding. With

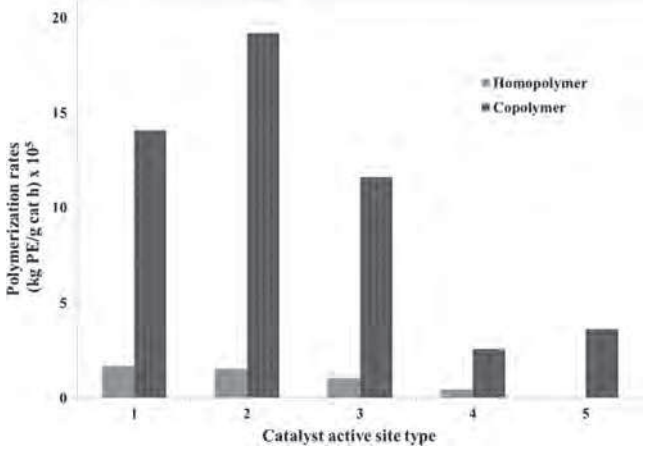

Figure 1. Catalyst active site type-dependent ethylene homo- and copolymerization with 1-hexene. The model-predicted homopolymerization rate for site type 5 is much smaller compared to that of copolymerization. Hence, it does not appear visible in the above figure.

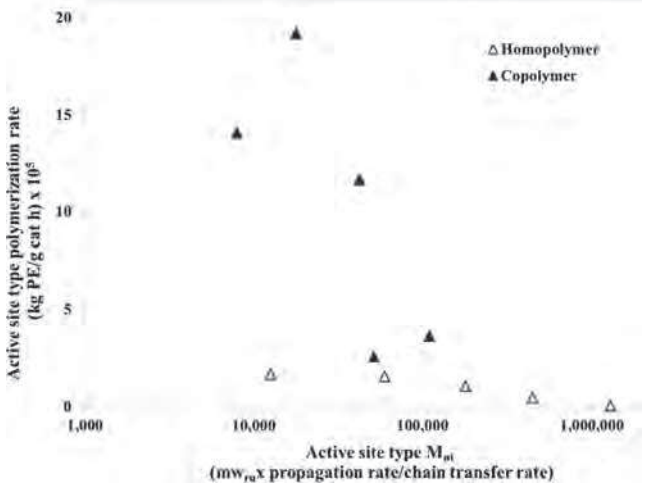

Figure 2. Relation between active site-specific polymerization rate and the corresponding number average molecular weight.

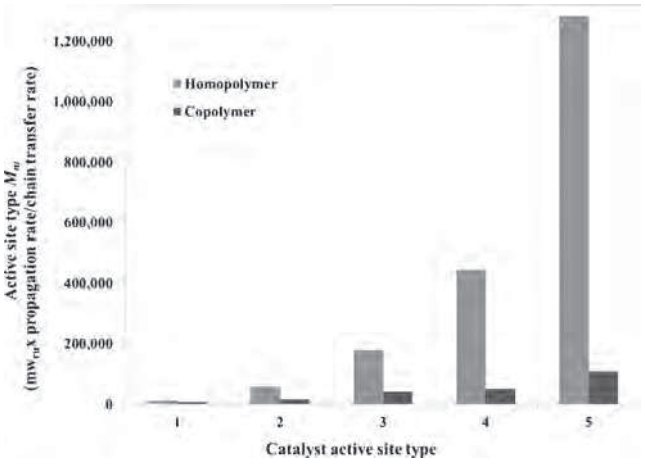

Figure 3. Comparison of catalyst active site-specific number average molecular weights of the as-synthesized ethylene homo- and copolymer.

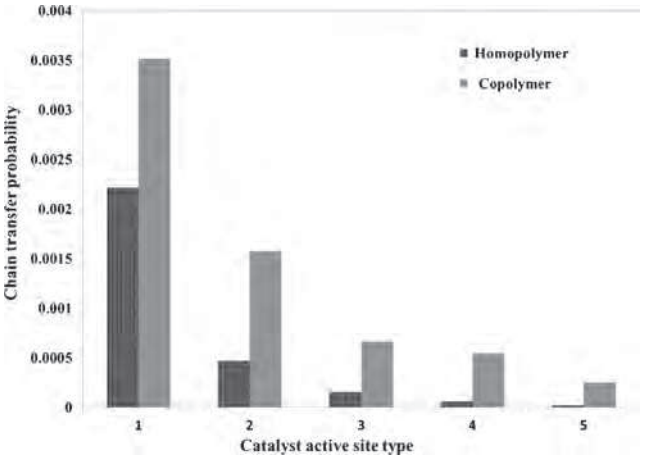

Figure 4. Comparison of catalyst active site-specific chain transfer probabilities during ethylene homo- and copolymerization trials.

reference to Appendix A (Equations A26 and A33), for a given active site type, we can write the following:

$$\frac{1}{M_{n,copolym}} > \frac{1}{M_{n,homopolym}}; \frac{1}{l_{n,copolym}} > \frac{1}{l_{n,homopolym}} \tag{1}$$

$$\frac{\left(k_{tr,\,\beta-H\to M_2}^{vinyl} + k_{tr2,\,\beta-H\to Zr^+}^{t-vinylene} + k_{tr,\,\beta-H\to Zr^+}^{vinyledene}\right) k_1}{\left(k_{p12}k_1\right) r_1 \frac{[M_1]}{[M_2]} + \left(\frac{k_{p11}k_1}{r_1} + \frac{k_{p22}k_2}{r_2}\right) + \left(k_{p21}k_2\right) r_2 \frac{[M_2]}{[M_1]}} > \frac{k_{tr,\,\beta-H\to M_1}^{vinyl}}{k_{p11}} + \frac{k_{tr,\,\beta-H\to Zr^+}^{vinyl} + k_{tr1,\,\beta-H\to Zr^+}^{t-vinylene}}{k_{p11}} \times \frac{1}{[M_1]} + \frac{k_{tr,\,\beta-H\to M_3}^{vinyledene}}{k_{p11}} \times \frac{[M_3]}{[M_1]} \tag{2}$$

The above expressions show how the active site type-dependent chain transfer phenomenon is influenced by the *apparent rate constants* of different termination reactions and the monomer concentrations.

Here, we revisit the aforesaid catalyst site type-dependent decrease in M_{ni} due to 1-hexene (acting as the chain transfer agent) from the perspective of the related chain transfer probability p_{CT_i}. (figure 4) (bar plot of p_{CT_i} versus site type). The objective is to more meaningfully explain this finding and the resulting implications. We calculated p_{CT_i} using Equation 4, which is derived below.

Using the relation $\frac{Termination\ rate}{Propagation\ rate} = \frac{mw_{ru}}{M_{ni}} = \frac{1}{l_{ni}}$ for an active site type i where mw_{ru} is the molecular weight of the repeat unit, we can write the following:

$$\frac{Termination\ rate}{Propagation\ rate + Termination\ rate} = \frac{1}{1 + l_{ni}} \tag{3}$$

The left hand side of Equation 3 defines the chain transfer probability p_{CT_i}.[45] Hence, we can rewrite Equation 3 as follows:

$$p_{CT_i} = \frac{1}{1 + l_{ni}} \tag{4}$$

Therefore, figure 4 eventually shows how the decrease in M_{ni} (or l_{ni}) directly relates to chain transfer probability p_{CT_i}. Figure 5 interestingly establishes that $\log(M_{ni})$ is linearly related to $\log(p_{CT_i})$, for the homo- as well as the copolymer, as reported below.

$$log\left(p_{CT_i}\right) = log(28) - log(M_{ni}) \tag{5}$$

Now, we show that Equation 5 matches the corresponding theoretical expression. Using the relation

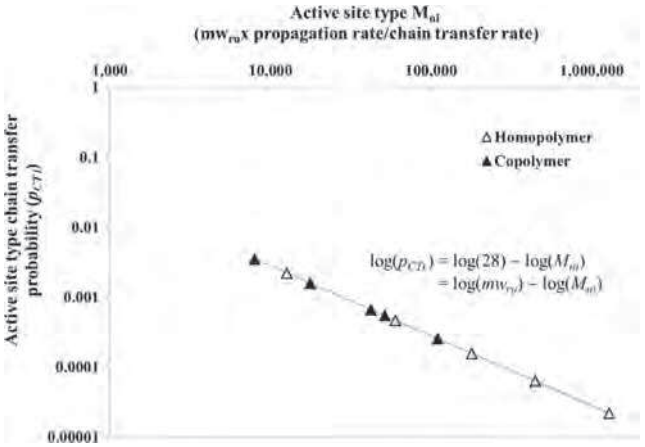

Figure 5. Relation between active site-specific chain transfer probability and the corresponding number average molecular weight.

$\frac{mw_{ru}}{M_{ni}} = \frac{1}{l_{ni}}$ and Equation 4, we can write the following:

$$log\left(p_{CT_i}\right) = log\left(mw_{ru}\right) - log\left(M_{ni}\left\{1 + \frac{mw_{ru}}{M_{ni}}\right\}\right) \quad (6)$$

In Equation 6, the term $\frac{mw_{ru}}{M_{ni}} \lll 1$. (table 3). Therefore, we can rewrite this equation as:

$$log\left(p_{CT_i}\right) = log\left(mw_{ru}\right) - log\left(M_{ni}\right) = log\,(28) - log\left(M_{ni}\right) \quad (7)$$

The above intriguing chain transfer feature (which has been developed considering the catalyst active centre distribution), to the best of our knowledge, has not been reported earlier in the literature. The significance of this logarithmic relation may be stated as follows.

The supported multiple equilibrium MAO-zirconocene ion pairs, with respect to each catalyst site type, differ in electronic and steric effects as well as coordination environments. This is why p_{CT_i}, in each case, is found to vary as a function of M_{ni} as illustrated above. However, why do the homo- and copolymerization results show the same logarithmic relation? This is because, with reference to the experimental supported catalyst and the given polymerization conditions, the following relation could be derived to hold:

$$\frac{\left(p_{CT_i}\right)_{copolym}}{\left(p_{CT_i}\right)_{homopolym}} = \frac{\left(M_{ni}\right)_{homopolym}}{\left(M_{ni}\right)_{copolym}} \quad (8)$$

Now, we discuss polymer backbone end unsaturations determined by FT-IR spectroscopy. The synthesized ethylene homopolymer showed terminal vinyl (CH_2 =CHR), *trans*-vinylene ($R_1CH{=}CHR_2$, $R_1 \neq R_2$), and vinyledene ($CH_2{=}CR_1R_2$, $R_1 \neq R_2$) unsaturations (table 2). The ratio of these unsaturations showed to be 1.000:7.244:0.433. This indicates that the concentrations of *trans*-vinylene and vinyledene unsaturations are the highest and the lowest, respectively. Therefore, this is the first study that reports the generation of all the above three unsaturations in supported metallocene-catalyzed ethylene homopolymer backbone. Note that, unsupported metallocenes, unlike the above, normally produce only terminal vinyl and *trans*-vinyl unsaturations.[4–11] Schemes I to III illustrate the mechanisms of formation of these backbone unsaturations, which we categorically summarize below.

The formation of terminal vinyl (CH_2 =CHR) is attributed to β-H transfer from the growing polymer backbone end to the incoming ethylene monomer and/or to the catalyst transition metal Zr (β-agostic interaction). In the first case, a metal ethyl ($Zr{-}C_2H_5$) species is produced while in the second case, a metal hydride (Zr−H) species is generated.[2–11] See Scheme I. These routes are kinetically distinguishable. The former is a bimolecular reaction with a sterically bulkier six-centred transition state. On the other hand, the latter is a unimolecular reaction having a four-centred transition state. Therefore, β-H transfer to the incoming monomer is more sensitive to steric environments around the catalyst active site than β-H transfer to Zr.[2]

Kinetically controlled chain isomerization followed by β-H transfer to ethylene generates *trans*-vinylene unsaturation ($R_1CH{=}CHR_2$, $R_1 \neq R_2$)[4–6,8,10] in the resulting homopolymer (Scheme II). Note that transfer of β-H prior to isomerization yields vinyl unsaturation. The chain isomerization has been reported in the literature to occur through the following steps:[5,6,8] (i) Transfer of β-H to the transition metal Zr, (ii) A partial detachment of the chain from Zr by breaking the Zr−CR bond (π-complexation), (iii) Relative rotation of the olefin and the metal hydride; and (iv) Reinsertion of hydrogen into the coordinated olefin, generating a structure with one primary and one secondary β-carbon.

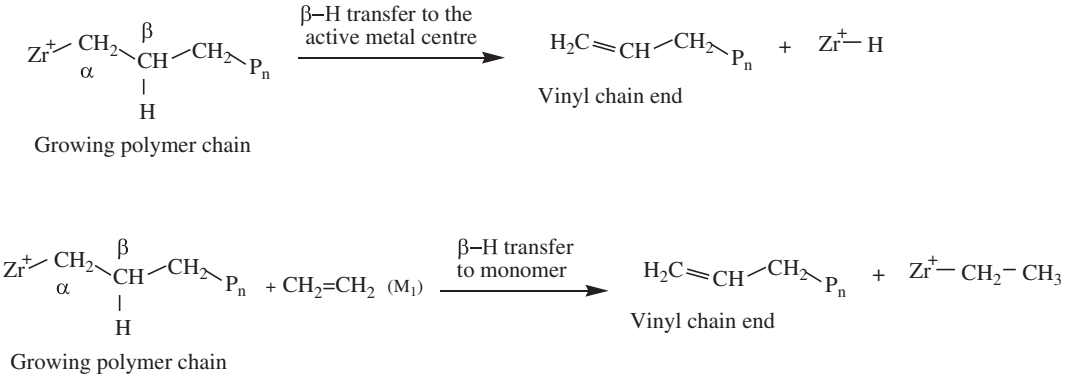

Scheme I. Generation of vinyl chain end in ethylene homopolymerization.

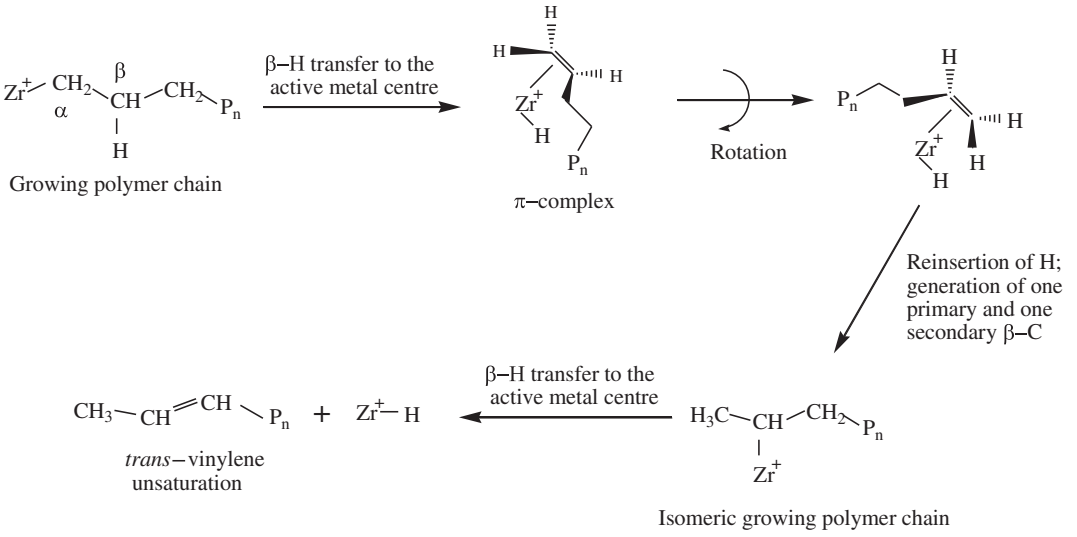

Scheme II. Generation of *trans*-vinyl chain end in ethylene homopolymerization.

The atypical vinyledene chain end ($CH_2=CR_1R_2$, $R_1 \neq R_2$) results from the re-insertion of an ethylene macromer into the growing polyethylene chain, followed by β-H transfer to ethylene monomer and/or to the catalyst transition metal (Scheme III).[10,46]

Now we discuss the chain end unsaturations in the synthesized copolymer. We observe that the copolymer, like the homopolymer, also showed all the three unsaturations—terminal vinyl, *trans*-vinylene, and vinyledene (table 2). The ratio of these unsaturations turned to be 1.000:5.617:15.900. This indicates that the concentrations of *trans*-vinylene and terminal vinyl unsaturations are the highest and the lowest, respectively. Additionally, we note that the total unsaturation of the copolymer is higher than that of the corresponding homopolymer. This matches what has been reported with reference to the growth of vinyledene and total unsaturations in ethylene-1-hexene copolymers, synthesized using unsupported metallocenes, in the literature.[2,9] Weight-average chain transfer probabilities of the homopolymer and the copolymers are 0.000238 and 0.000971, respectively. Scheme IV elucidates the mechanisms of generating the copolymer backbone unsaturations as per the following three routes:[43,44]

- **Route A:** With ethylene as the last inserted unit, β-hydrogen transfer to Zr^+ and/or to ethylene or 1-hexene generates vinyl terminus ($CH_2=CHR$).
- **Route B:** With ethylene as the last inserted unit, 2, 1 misinsertion of 1-hexene, followed by β-hydrogen elimination to the Zr^+ active sites generates *trans*-vinylene terminus ($R_1CH=CHR_2$; $R_1 \neq R_2$).
- **Route C:** With ethylene as the last inserted unit, 1, 2 insertion of 1-hexene generates vinylidene terminus ($CH_2=CR_1R_2$; $R_1 \neq R_2$) (through β-hydrogen elimination to Zr^+ active sites).

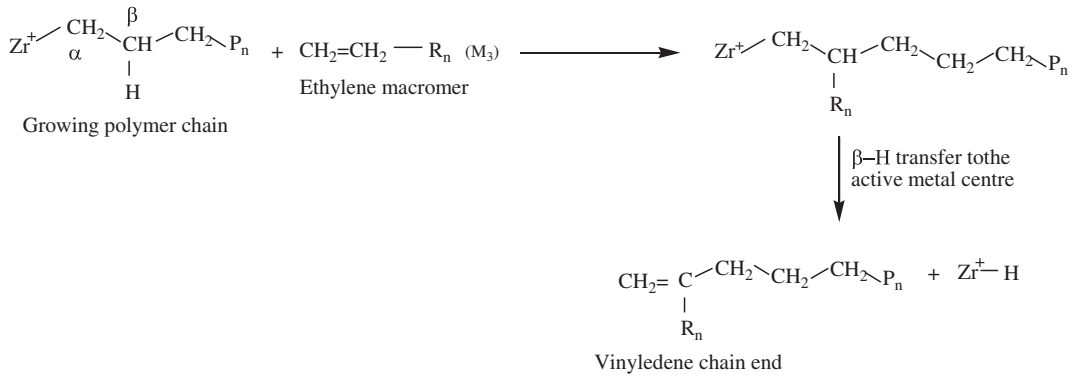

Scheme III. Generation of vinyledene chain end in ethylene homopolymerization.

Route A: Vinyl terminus

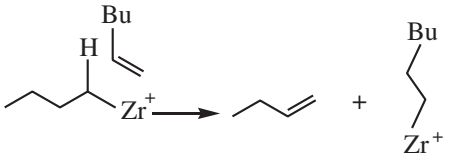

Route B: *trans*-Vinyl terminus

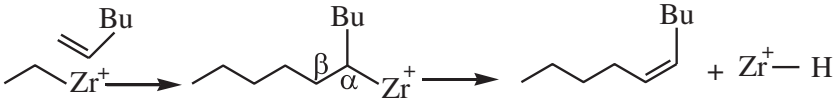

Route C: Vinylidene terminus

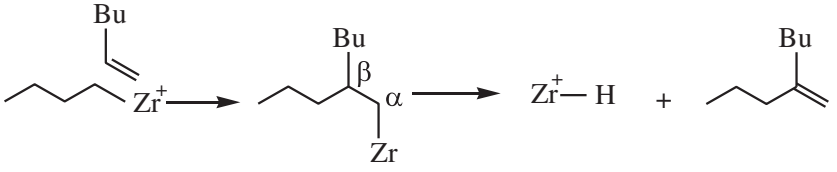

Scheme IV. Generation of vinyl, *trans*-vinyl, and vinyledene chain ends in ethylene-1-hexene copolymerization.

4. Conclusions

To increase the application of supported metallocenes for producing advanced grades of polyethylenes, the following two subjects, listed with the others, are very important. One is the effect of catalyst active centre distribution on chain termination reaction, which regulates the polymer molecular weight. The other is the backbone terminal vinyl unsaturaton that opens venues for post-modification. Therefore, we recently modelled the catalyst active centre distribution of a supported metallocene catalyst—(silica/MAO/(^{n}BuCp)$_2$ZrCl$_2$—by simultaneous deconvolution of the measured molecular weight and copolymer composition distributions of the resulting polyethylenes, and confirmed the model prediction experimentally (using the differential scanning calorimetry-based successive self-nucleation and annealing (SSA) technique) as well as from the perspective of MAO structural heterogeneity.[24,25] In this study, we applied the above model-predicted parameters to evaluate the active-centre-dependent ethylene homo- and copolymerization rates, as well as the corresponding chain termination rates. This enabled us to study 1-hexene-induced positive comonomer effect and chain transfer phenomenon from a microkinetic mechanistic viewpoint, which, to the best of our knowledge, has not been published earlier. In this regard, we particularly conclude the following:

- The active site type-dependent homo- and copolymerization rates were fairly inversely related to the respective number average molecular weights.
- The kinetic expressions, developed on the basis of the proposed polymerization mechanisms, better illustrated how the active site type-dependent chain transfer phenomenon is influenced by the different apparent termination rate constants and the momoner concentration(s).
- The application of the concept of chain transfer probability p_{CT_i} successfully explained why the copolymer total chain end unsaturation exceeded that of the homopolymer, and showed how active centre-specific molecular weight M_{ni} decreased as per the following expression:

$$log\left(p_{CT_i}\right) = log\left(mw_{ru}\right) - log\left(M_{ni}\right) = log\,(28) - log\left(M_{ni}\right)$$

- All the three chain end unsaturations—vinyl, vinylende, and trans-vinylene—were noted in the ethylene homo- and copolymer backbones, synthesized by the supported (^{n}BuCp)$_2$ZrCl$_2$ catalyst. Note that unsupported metallocenes, unlike the above, normally produce only terminal vinyl and *trans*-vinyl

unsaturations.[4–11] Mechanisms have been postulated to reveal the underlying polymer chemistry.

- The present findings will help design and synthesize future supported metallocene catalysts, capable of better regulating the copolymer backbone compositional variations and the associated chain end unsaturations. Consequently, it will be possible to better prepare functional polyolefins using such metallocene polyethylene precursors.

Acknowledgements

The authors acknowledge the financial support provided by King Abdulaziz City for Science and Technology (KACST) via the Science & Technology Unit at King Fahd University of Petroleum & Minerals (KFUPM) through Project Number 08-PET90-4 as part of the National Science and Technology Innovation Plan. The technical assistance provided by Center of Refining & Petrochemicals (CRP), Dhahran, Saudi Arabia; NMR Core Laboratory, Thuwal, King Abdullah University of Science & Technology (KAUST), Saudi Arabia; and the Department of Chemical Engineering at KFUPM and the Department of Chemical Engineering at Kasetsart University, Thailand is also gratefully acknowledged. Messrs. Anwar Hossaen and Sarath P. Unnikari are thanked for technical support. The gift of 1-hexene by United Petrochemicals, Al-Jubail is highly appreciated.

Appendix A: Kinetic Derivation

We begin the kinetic derivation by considering the fact that the MAO cocatalyst first monomethylates one of the chloride ligands attached to transition metal (Zr). Next, it abstracts the chloride ligand to generate the active metallocenium cation (Zr^+).[17,19,30–37] See Equation A1. Reversible complex formation[11,38–41] with the transition metal active site, as per the *trigger mechanism* of Ystenes,[42] is a pre-requisite to propagation. See Equations A2 and A3. As per Ystenes, the coordination site is never free; it is always occupied by a monomer. This complexed monomer gets inserted into the growing polymer chain as soon as another incoming monomer is ready to complex through expansion of the coordination sphere. This associates two monomers with the active centre in the form of a transition state.[37] Equations A4 to A7 represent the post-complexation four-step propagation reactions.

Activation:

$$Zr + MAO \xrightarrow{k_i} Zr^+ (metallocenium\ cation) + MAO^- \tag{A1}$$

Reversible complex formation:

$$Zr^+ + M_1 \underset{k_{r1}}{\overset{k_{f1}}{\rightleftharpoons}} Zr^+ \ldots M_1 \tag{A2}$$

$$Zr^+ + M_2 \underset{k_{r2}}{\overset{k_{f2}}{\rightleftharpoons}} Zr^+ \ldots M_2 \tag{A3}$$

Propagation:

$$P_n^{M_1} - Zr^+ + M_1 \xrightarrow{k_{p11}} P_{n+1}^{M_1} - Zr^+ \tag{A4}$$

$$P_n^{M_1} - Zr^+ + M_2 \xrightarrow{k_{p12}} P_n^{M_1} - M_2 - Zr^+ \tag{A5}$$

$$P_n^{M_2} - Zr^+ + M_2 \xrightarrow{k_{p22}} P_{n+1}^{M_2} - Zr^+ \tag{A6}$$

$$P_n^{M2} - Zr^+ + M_1 \xrightarrow{k_{p21}} P_n^{M_2} - M_1 - Zr^+ \tag{A7}$$

The effective ethylene homopolymerization chain transfer reactions, according to Schemes I to III (developed as per the backbone end saturations, determined in this study, by FTIR spectroscopy), and citation in the literature,[2,4–10] can be written as follows:

$$P_n^{M_1} - Zr^+ + M_1\,(CH_2 = CH_2) \xrightarrow{k_{tr,\,\beta-H\to M_1}^{vinyl}} \overset{\equiv}{P}_{n,vinyl} + Zr^+ - CH_2 - CH_3 \tag{A8}$$

$$P_n^{M_1} - Zr^+ \xrightarrow{k_{tr,\,\beta-H\to Zr^+}^{vinyl}} \overset{\equiv}{P}_{n,vinyl} + Zr^+ - H \tag{A9}$$

$$P_n^{M_1} - Zr^+ \xrightarrow{k_{tr1,\,\beta-H\to Zr^+}^{t-vinylene}} \overset{\equiv}{P}_{n,t-vinylene} + Zr^+ - H \tag{A10}$$

$$P_n^{M_1} - Zr^+ + M_3\,(macromer) \xrightarrow{k_{tr,\,\beta-H\to M_3}^{vinyledene}} \overset{\equiv}{P}_{n,vinyledene} + Zr^+ - H \tag{A11}$$

Similarly, the effective ethylene-1-hexene copolymerization chain transfer reactions, according to Scheme IV (developed as per the backbone end saturations, determined in this study, by FTIR spectroscopy), and citation in the literature,[43,44] can be listed as:

$$P_n^{M_1} - Zr^+ + M_2(CH_2 = CH - Bu) \xrightarrow{k_{tr,\,\beta-H\to M_2}^{vinyl} + (Route\ A)} \overset{\equiv}{P}_{n,vinyl} + Zr^+ - H \tag{A12}$$

$$P_n^{M_1} - Zr^+ + M_2(CH_2 = CH - Bu) \xrightarrow{k_{tr2,\ \beta-H\to Zr^+}^{t-vinylene}(Route\ B)} \overset{\equiv}{P}_{n,t-vinylene} + Zr^+ - H \quad (A13)$$

$$P_n^{M_1} - Zr^+ + M_2(CH_2 = CH - Bu) \xrightarrow{k_{tr,\ \beta-H\to Zr^+}^{vinyledene}(Route\ C)} \overset{\equiv}{P}_{n,vinyledene} + Zr^+ - H \quad (A14)$$

From Equations A2 and A3, as per steady state assumption, we can write the following:

$$\frac{d\left[M_1 - Zr^+\right]}{dt} = k_{f_1}\left[Zr^+\right][M_1] - k_{r_1}\left[M_1 - Zr^+\right] = 0 \quad (A15)$$

$$\frac{d\left[M_2 - Zr^+\right]}{dt} = k_{f_2}\left[Zr^+\right][M_2] - k_{r_2}\left[M_2 - Zr^+\right] = 0 \quad (A16)$$

According to long chain hypothesis, we next derive the following:

$$\left[M_1 - Zr^+\right] = \left[P_n^{M_1} - Zr^+\right] = \frac{k_{f_1}}{k_{r_1}}\left[Zr^+\right][M_1] = k_1\left[Zr^+\right][M_1]; \quad k_1 = \frac{k_{f_1}}{k_{r_1}} \quad (A17)$$

$$\left[M_2 - Zr^+\right] = \left[P_n^{M_2} - Zr^+\right] = \frac{k_{f_2}}{k_{r_2}}\left[Zr^+\right][M_2] = k_2\left[Zr^+\right][M_2]; \quad k_2 = \frac{k_{f_2}}{k_{r_2}} \quad (A18)$$

At small time scale, the total concentration of active sites is constant. Therefore, we can write:

$$C_t = \left[Zr^+\right] + \left[P_n^{M_1} - Zr^+\right] + \left[P_n^{M_2} - Zr^+\right] \quad (A19)$$

Using Equations A17 to A19, we can write the following:

$$\left[Zr^+\right](uncomplexed) = \frac{1}{1 + k_1[M_1] + k_2[M_2]} \times C_t \quad (A20)$$

$$\left[P_n^{M_1} - Zr^+\right](complexed) = \frac{k_1[M_1]}{1 + k_1[M_1] + k_2[M_2]} \times C_t \quad (A21)$$

$$\left[P_n^{M_2} - Zr^+\right](complexed) = \frac{k_2[M_2]}{1 + k_1[M_1] + k_2[M_2]} \times C_t \quad (A22)$$

Now, we deduce the desired kinetic rate expressions for ethylene homopolymerization. Using Equations A4 and A21, we can write the following expressions:

$$C_{t,homopolym} = \left[Zr^+\right] + \left[P_n^{M_1} - Zr^+\right];\ [M_2] = 0 \quad (A23)$$

$$R_{p,homopolym} = -\frac{d[M_1]}{dt} = k_{p11}\left[P_n^{M_1} - Zr^+\right][M_1] = \frac{k_{p11}k_1[M_1]^2}{1 + k_1[M_1]} \times C_{t,homopolym} \quad (A24)$$

Considering Equations A8 to A11, and A21, we write ethylene homopolymerization termination rate as follows:

$$R_{tr,homopolym} = \left(k_{tr,\ \beta-H\to M_1}^{vinyl}[M_1] + k_{tr,\ \beta-H\to Zr^+}^{vinyl} + k_{tr1,\ \beta-H\to Zr^+}^{t-vinylene} + k_{tr,\ \beta-H\to M_3}^{vinyledene}[M_3]\right) \times \frac{k_1[M_1]}{1 + k_1[M_1]} \times C_{t,homopolym} \quad (A25)$$

Using $\frac{mw_{ru}}{M_{n,homopolym}} = \frac{R_{tr,homopolym}}{R_{p,homopolym}} = \frac{1}{l_{n,homopolym}}$, and Equations A23 and A24, we write the following final expression:

$$\frac{1}{l_{n,homopolym}} = \frac{k_{tr,\ \beta-H\to M_1}^{vinyl}}{k_{p11}} + \frac{k_{tr,\ \beta-H\to Zr^+}^{vinyl} + k_{tr1,\ \beta-H\to Zr^+}^{t-vinylene}}{k_{p11}} \times \frac{1}{[M_1]} + \frac{k_{tr,\ \beta-H\to M_3}^{vinyledene}}{k_{p11}} \times \frac{[M_3]}{[M_1]} \quad (A26)$$

Next, we develop the final expression for $\frac{1}{l_{n,copolym}}$. In this regard, considering Equations A4 to A7, we write the copolymerization rates for M_1 and M_2 as follows:

$$R_{p_1} = -\frac{d[M_1]}{dt} = k_{p11}\left[P_n^{M_1} - Zr^+\right][M_1] + k_{p21}\left[P_n^{M_2} - Zr^+\right][M_1] \quad (A27)$$

$$R_{p2} = -\frac{d[M_2]}{dt} = k_{p22}\left[P_n^{M_2} - Zr^+\right][M_2] + k_{p12}\left[P_n^{M_1} - Zr^+\right][M_2] \quad (A28)$$

Using Equations A21 and A22, we write the above equations, respectively, as follows:

$$R_{p_1} = \frac{k_{p11}k_1[M_1]^2 + k_{p21}k_2[M_1][M_2]}{1 + k_1[M_1] + k_2[M_2]} \times C_t \quad (A29)$$

$$R_{p_2} = \frac{k_{p22}k_2[M_2]^2 + k_{p12}k_1[M_1][M_2]}{1 + k_1[M_1] + k_2[M_2]} \times C_t \quad (A30)$$

Eqs. A29 and A30 lead to the following:

$$R_{p,copolym} = \frac{k_{p11}\,k_1\,[M_1]^2 + \left(k_{p21}\,k_2 + k_{p12}\,k_1\right)[M_1]\,[M_2] + k_{p22}\,k_2\,[M_2]^2}{1 + k_1\,[M_1] + k_2\,[M_2]} \times C_t \tag{A31}$$

Applying Equations A12 to A14, and A21, we can write the overall copolymerization termination rate as follows:

$$R_{tr,copolym} = \left(k^{vinyl}_{tr,\ \beta-H\rightarrow M_2} + k^{t-vinylene}_{tr2,\ \beta-H\rightarrow Zr^+} + k^{vinyledene}_{tr,\ \beta-H\rightarrow Zr^+}\right) \times \frac{k_1\,[M_1]\,[M_2]}{1 + k_1\,[M_1] + k_2\,[M_2]} \times C_t \tag{A32}$$

Using Equations A29 and A30, we finally write:

$$\frac{1}{l_{n,copolym}} = \frac{\left(k^{vinyl}_{tr,\ \beta-H\rightarrow M_2} + k^{t-vinylene}_{tr2,\ \beta-H\rightarrow Zr^+} + k^{vinyledene}_{tr,\ \beta-H\rightarrow Zr^+}\right) k_1}{\left(k_{p12}\,k_1\right) r_1 \frac{[M_1]}{[M_2]} + \left(\frac{k_{p11}\,k_1}{r_1} + \frac{k_{p22}\,k_2}{r_2}\right) + \left(k_{p21}\,k_2\right) r_2 \frac{[M_2]}{[M_1]}} \tag{A33}$$

where $r_1 = \frac{k_{p11}}{k_{p12}}$ and $r_2 = \frac{k_{p22}}{k_{p21}}$ are the reactivity ratios of M_1 and M_2, respectively.

Note that under the present situation, the concentration of a given active site type is not known. Therefore, all the aforesaid rate constants should be considered to be *apparent* rate constants.

References

1. Atiqullah M, Tinkl M, Pfaendner R, Akhtar M N and Hussain I 2010 *Polym. Rev.* **50** 178
2. Terao H, Ishii S, Saito J, Matsuura S, Mitani M, Nagai N, Tanaka H and Fujita T 2006 *Macromolecules* **39** 8584
3. Atiqullah M, Winston M S, Bercaw J E, Hussain I, Fazal A, Al-Harthi M A, Emwas A H M, Khan M J and Hossaen A 2012 *Polym. Degrad. Stab.* **97** 1164
4. Thorshaug K, Rytter E and Ystenes M 1997 *Macromol. Rapid. Commun.* **18** 715
5. Thorshaug K, Støvneng J A, Rytter E and Ystenes M 1998 *Macromolecules* **31** 7149
6. Thorshaug K, Støvneng J A, Rytter E and Ystenes M 2000 *Macromolecules* **33** 8136
7. Wigum H, Tangen L, Støvneng J A and Rytter E 2000 *J. Polym. Sci: Part A: Polym. Chem.* **38** 3161
8. Lehmus P, Kokko E, Leino R, Luttikhedde H J G, Rieger B and Seppala J V 2000 *Macromolecules* **33** 8534
9. Bruaseth I, Bahr M, Gerhard D and Rytter E 2005 *J. Polym. Sci: Part A: Polym. Chem.* **43** 2584
10. Białek M 2010 *J. Polym. Sci: Part A: Polym. Chem.* **48** 3209
11. Mehdiabadi S and Soares J B P 2012 *Macromolecules* **45** 1777
12. Wang W-J, Zhu S and Park S-J 2000 *Macromolecules* **33** 5770
13. Webb S W, Weist E L, Chiovetta M G, Laurence R L and Conner W C 1991 *Can. J. Chem. Eng.* **69** 665
14. Martino A D, Broyer J P, Spitz R, Weickert G and McKenna T F L 2005 *Macromol. Rapid Commun.* **26** 215
15. Silva F M, Broyer J P, Novat C, Lima E L, Pinto J C and McKenna T F L 2005 *Macromol. Rapid Commun.* **26** 1846
16. Martino A D, Weickert G, Sidoroff F and McKenna T F L 2007 *Macromol. React. Eng.* **1** 338
17. Severn J R and Chadwick J C 2008 In *Tailor-made Polymers: 578 Via Immobilization of Alpha-olefin Polymerization Cat- 579 alysts* (Weinheim: Wiley-VCH) p. 113
18. Choi Y and Soares J B P 2012 *Can. J. Chem. Eng.* **90** 646
19. Atiqullah M, Akhtar M N, Moman A A, Abu-Raqabah A H, Palackal S J, Al-Muallem H A and Hamed O M 2007 *Appl. Catal. A: Gen.* **320** 134
20. Białek M and Czaja K 2006 *Macromol. Chem. Phys.* **207** 1651
21. Grieken R V, Carrero A, Suarez I and Paredes B 2007 *Macromol. Symp.* **259** 243
22. Lee J S, Yim J H, Jeon J K and Ko Y S 2012 *Catal. Today* **185** 175
23. Akhtar M N, Atiqullah M, Moman A A, Abu-Raqabah A H and Ahmed N 2008 *Macromol. React. Eng.* **2** 339
24. Atiqullah M, Anantawaraskul S, Emwas A M, Al-Harthi M A, Hussain I, Ul-Hamid A and Hossaen A 2013 *Ind. Eng. Chem. Res.* **52** 9359
25. Atiqullah M, Cibulková Z, Černá A, Šimon P, Hussain I, Al-Harthi M A and Anantawaraskul S 2014 *J. Therm. Anal. Calori.* **119**(1) 581
26. Soares J B P 2007 *Macromol. Symp.* **257** 1
27. Alghyamah A A and Soares J B P 2009 *Macromol. Rapid Commun.* **30** 384
28. Anantawaraskul S, Bongsontia W and Soares J B P 2011 *Macromol. React. Eng.* **8** 549
29. Soares J B P and Hamielec A E 1995 *Polymer* **36** 2257
30. Wang Q, Song L and Zhao Y L 2001 *Macromol. Rapid Commun.* **22** 1030
31. Zurek E A 2002 In *Theoretical Investigation of the Structure 608 and Function of MAO* (Canada: University of Calgary) 609 p. 57
32. Negureanu L, Hall R W, Butler L G and Simeral L A 2006 *J. Am. Chem. Soc.* **128** 16816
33. Linnolahti M, Severn J R and Pakkanen T A 2008 *Angew Chem. Int. Ed.* **47** 9279
34. Ystenes M, Eilertsen J L, Jianke L I U, Matthias O H, Rytter E and Stovneng J A 2000 *J. Polym. Sci. Part A: Polym. Chem.* **38** 3106
35. Talsi E P, Semikolenova N V, Panchenko V N, Sobolev A P, Babushkin D E, Shubin A A and Zakharov V A 1999 *J. Mol. Catal. A: Chem.* **139** 131
36. Boudene Z, De Bruin T, Toulhoat H and Raybaud P 2012 *Organometallics* **31** 8312

37. Huang J and Rempel G L 1995 *Prog. Polym. Sci.* **20** 459
38. Bohm L L 1984 *J. Appl. Polym. Sci.* **1** 279
39. Shaffer W and Ray W J 1997 *J. Appl. Polym. Sci.* **6** 1053
40. Schnuss A and Reichert K 1990 *Makromol. Chem. Rapid Commun.* **7** 315
41. Bergstra M F and Günter W 2005 *Macromol. Mater. Eng.* **290** 610
42. Ystenes M 1991 *J. Catal.* **129** 383
43. Ystenes M 1993 *Makromol. Chem. Macromol. Symp.* **66** 71
44. DesLauriers P J, Tso C, Youlu Yu, Rohlfing D L and McDaniel M P 2010 *Appl. Catal. A: Gen.* **388** 102
45. Killian C M, Johnson L K and Brookhart M 1997 *Organometallics* **16** 2005
46. Dang V A, Yu L C, Balboni D, Dall'Occo T, Resconi L, Mercandelli P, Moret M and Sironi A 1999 *Organometallics* **18** 3781